A Phase Synchronization Technique for Multistatic SAR Systems Based on a Microwave Link

Nertjana Ustalli
Microwaves and Radar Institute
German Aerospace Center (DLR)
Weßling, Germany
nertjana.ustalli@dlr.de

Gerhard Krieger
Microwaves and Radar Institute
German Aerospace Center (DLR)
Weßling, Germany
gerhard.krieger@dlr.de

Josef Mittermayer
Microwaves and Radar Institute
German Aerospace Center (DLR)
Weßling, Germany
Josef.Mittermayer@dlr.de

Michelangelo Villano
Microwaves and Radar Institute
German Aerospace Center (DLR)
Weßling, Germany
michelangelo.villano@dlr.de

***Abstract*—Phase synchronization poses a significant challenge for multistatic synthetic aperture radar (SAR) systems. A novel concept called MirrorSAR has been introduced, which relies on a configuration of transmitter and receiver satellites positioned at separate locations. In this setup, the receiver satellites serve as mirrors or space transponders, redirecting the radar echoes back to the transmitter. This arrangement simplifies the receiver functionality and enables the utilization of cost-effective platforms, particularly in the emerging NewSpace domain. Within the transmitter, the forwarded radar signals are coherently demodulated using the same oscillator responsible for generating the radar pulses. This eliminates the need for a bidirectional phase synchronization link between the transmitter and receiver, as observed in TanDEM-X, thus allowing for innovative synchronization approaches that aims to guarantee the bistatic and interferometric performance while keeping the receiver complexity low. This paper further improves the phase synchronization approach based on a microwave link within the MirrorSAR concept. The phase synchronization accuracy is assessed from simulation based on real TerraSAR-X data.**

Keywords—Bistatic radar, interferometry, MirrorSAR, multistatic radar, phase noise, small satellites, synchronization, synthetic aperture radar (SAR).

I. Introduction

Synthetic aperture radar (SAR) is a remote sensing technology widely used for Earth observation applications. SAR enables efficient operation in adverse weather conditions where visible/infrared systems would be impractical. It can penetrate clouds, haze, rain, fog, and precipitation with minimal signal attenuation. Additionally, as an active sensor with its own source of illumination, SAR can operate both day and night [1].

In recent years, there has been a growing interest in bi- and multistatic SAR systems [2]-[4], which present various opportunities compared to their monostatic counterparts, including frequent monitoring, high-resolution wide-swath imaging, improved scene classification through bistatic imaging, generation of high-resolution digital elevation models (DEMs) with decimeter-level height accuracy using multibaseline cross-track interferometry, SAR tomography, as well as enhanced flexibility and reliability. However, the implementation of these systems introduces new challenges that need to be addressed, such as collision avoidance within closely spaced satellite formations, orbit design to establish appropriate baselines, instrument synchronization encompassing time, space, and phase synchronization, and considerations for cost reduction [5]-[16].

Among the aforementioned challenges, phase synchronization is one of the most critical. Because the radar oscillators in bistatic and multistatic SAR systems are separated, the relative frequency deviation and phase noise between the transmitting and receiving oscillators cannot be canceled as in monostatic SAR, which uses the same oscillator for modulation and demodulation. Uncompensated phase errors in case of bistatic SAR may cause not only a distortion of bistatic SAR focusing (i.e., time variant shift, spurious side lobes, and a broadening of the impulse response, as well as low-frequency phase modulation of the focused SAR signal), but also interferometric phase errors, which can result in a low-frequency modulation of the DEM along azimuth [12].

Ensuring interferometric phase stability imposes strict requirements, necessitating relative phase referencing between independent ultrastable oscillators. In recent years, several studies on phase referencing for bistatic SAR systems have been published [9]-[16]. For example, a pulsed alternate synchronization method was proposed in [13] and was subsequently successfully used in TanDEM-X [17]. An alternative to such relative phase referencing solutions is the use of hyperstable oscillators in conjunction with ground control points [12].

MirrorSAR, an innovative SAR system concept introduced in [18]-[19], comprises a set of spatially separate transmit and receive satellites and employs a fractioned radar architecture to mitigate the complexity, weight, and power demands of the receiver hardware. MirrorSAR presents a promising approach for implementing cost-effective yet high-performance multistatic SAR missions, particularly within the NewSpace context. It can be operated in various modes, including single-transmit single-receive mode, single-transmit multiple-receive mode (as shown in Fig. 1), or even multiple-transmit multiple-receive mode. The scene is illuminated by the transmitting satellite and the backscattered radar signals received by the receiving satellites are forwarded towards the transmitter through a phase preserving link. The routed radar signals are then demodulated to baseband by using, for example, a coherent I/Q demodulator driven by the local oscillator of the transmitter. As this oscillator has also

This work was partially funded by the European Union (ERC, DRITUCS, 101076275). Views and opinions expressed are however those of the authors only and do not necessarily reflect those of the European Union or the European Research Council Executive Agency. Neither the European Union nor the granting authority can be held responsible for them.

been used to generate the transmitted radar pulse, possible frequency and phase drifts are canceled, as in a classical monostatic SAR.

In the initial phase (Phase 0/A) of the HRWS mission, the Microwaves and Radar Institute of DLR suggested expanding the mission by incorporating three compact and cost-effective receive-only satellites utilizing the MirrorSAR concept [20]-[21]. This innovative approach of MirrorSAR facilitates simultaneous acquisition of various large and small Rx baselines, enabling precise and reliable SAR interferometry. The mission aims to deliver a worldwide X-band DEM with a height accuracy of 2 m (point-to-point error, 90% confidence interval) and a horizontal resolution of 4 m × 4 m [22].

A crucial aspect of MirrorSAR is bistatic radar signal synchronization. Two different synchronization approaches were presented in [18]-[19], aiming to maintain a low receiver complexity while ensuring the desired bistatic and interferometric performance.

The first synchronization approach entails the employment of a modulation that preserves the phase of the forwarded radar signal and avoids any dependency on the phase of the modulation carrier. For example, the receiver satellite generates a high frequency signal, which can be either microwave or an optical carrier, which is then amplitude modulated by the radar echo before being forwarded to the transmitter. A simple amplitude demodulation at the transmitter can recover the time-delayed radar echo without phase disturbance from the high frequency carrier. Subsequently, the radar echoes are demodulated to baseband using the same oscillator utilized for generating the transmitted radar pulses. An alternative approach for achieving the required phase synchronization, is the utilization of a microwave link. In this approach, a synchronization signal is transmitted from the transmitting satellite towards the receiving satellites via a dedicated low-gain antenna. The received synchronization signal is superimposed to the radar echo on the receiving satellite and subsequently forwarded to the transmitter satellite. The demodulation to baseband is performed by using the same oscillator used to generate transmitted radar pulses. This methodology ensures that any additional phase errors introduced on either the receiver or transmitter side will be identical for both the mirrored synchronization signal and the radar signal. An assessment of the synchronization signal enables the compensation of these phase errors in the radar echo.

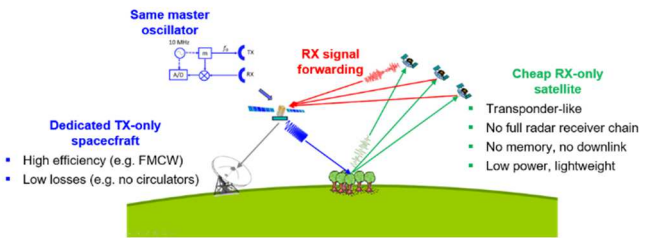

Fig. 1 (Reproduced from [18]) Illustration of the MirrorSAR concept. The scene is illuminated by the transmitter satellites. The scattered radar waves are then received by multiple receivers that route their recorded signals to the transmitter. The transmitter satellite then coherently demodulates the forwarded signals before transferring them to the ground.

The latest approach still leaves some open issues:

(i) The synchronization signal received by the Rx satellite needs to be weaker to avoid affecting the radar echo from the ground, while still ensuring accurate phase error estimation of less than 1° for interferometric applications.

(ii) Separating the synchronization signal from the radar echoes can be achieved in the range-Doppler domain. However, due to the varying distance between the Tx and Rx satellites during data collection, the Doppler frequency of the synchronization signal will not be zero, necessitating accurate knowledge of the Doppler frequency.

(iii) The process of removing the synchronization signal should minimally or not at all impact the radar echo from the ground.

In light of the aforementioned open issues, this paper further improves the phase synchronization approach based on a microwave link by estimating the phase errors from the synchronization signal, even for low power values (i.e., -7 dB below the received radar echo's power), and subsequently removing it with minimal impact on the radar echoes.

II. Synchronization Concept Based on a Microwave Link

In this section the synchronization concept based on microwave link will be introduced using the flowchart in Fig. 2 and a stepwise description. First, an overview of the synchronization technique will be presented, divided into two parts: on-board and on-ground. We will introduce the fundamental building blocks of each part. Afterward, each block of the synchronization concept will be refined in greater depth.

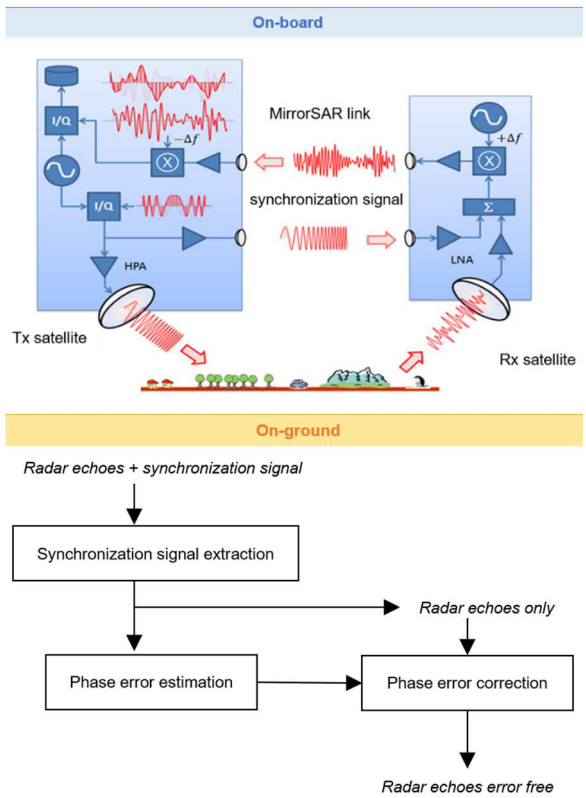

Fig. 2 Main building blocks of the microwave link-based synchronization approach: (upper panel) on-board and (bottom panel) on-ground.

The on-board synchronization for the case of a bistatic SAR system is shown in the upper panel of Fig. 2. A synchronization signal is sent from Tx satellite to the Rx satellite. The synchronization signal is received in the Rx

satellite by a dedicated antenna and superimposed then to the radar echo. In the Rx satellite, the overlaid signals are jointly frequency shifted by $+\Delta f$ using a coherent mixer and then radiated back to the transmitter. The superimposed shifted signal is received by the Tx satellite. Then, the additional frequency shift is reversed before the signal is down-converted to baseband using the transmitter's local oscillator (LO). Finally, the baseband signal that is the sum of the radar echo and synchronization signal is digitized, stored in memory, and transmitted to the ground.

The superimposed synchronization signal and radar echo must be separated on the ground. It should be noted that the independent Rx satellite up-conversion, i.e., $+\Delta f$, and the Tx satellite down-conversion, i.e., $-\Delta f$ (see upper panel of Fig. 2) introduce phase errors. However, these phase errors are the same for both the mirrored synchronization signal and the radar echo. As a result, after separating the synchronization signal from the radar echoes, an evaluation of the synchronization signal allows for the estimation and subsequently correction of these phase errors on the radar echo, as illustrated in the bottom panel of Fig. 2. The synchronization signal will be removed from the radar echoes while attempting not to impact them.

Each component of the synchronization technique will now be discussed in greater depth, along with challenges and potential solutions, beginning with the on-board part and progressing to the on-ground part.

A. On-board

The synchronization signal transmitted from Tx satellite towards Rx satellite can be a copy of the radar pulses sent to ground or a dedicated waveform that is coherently derived from the transmitters ultra-stable oscillator. It is important to note that in order to avoid the saturation on the receiver side the synchronization signal will be weaker than the received radar echo. For every transmitted pulse on the ground we transmit a synchronization signal towards the Rx satellite with an additional delay (e.g., via a delay line or, more simply, by a cable whose length exceeds the final range resolution) in order to avoid potential interference issues between the radar pulse sent to the ground and the much weaker synchronization signal sent to the receiver [18]. This interference could distort and shift the phase of the synchronization signal. In this way, the unintended direct signal radiated from the main radar antenna and the desired synchronization signal transmitted via the dedicated space-to-space link can be mutually separated in ground processing.

The synchronization signal will be received by the Rx satellite after a time delay that depends on the distance between the Tx and Rx satellite, d_{Tx-Rx}, and the radar echo from the ground will be received after a time delay that depends on the bistatic range, r_{bi}. Due to the different time delays a number of pulses equal to the number of traveling pulses (the number of pulses transmitted before the echo of any given pulse is received) will only have the synchronization signal returns, so these pulses will be shifted in frequency of $+\Delta f$ and forwarded to the Tx satellite without the superimposed radar echo returns. The number of traveling pulses is given by:

$$N_{synch_{only}} = \left\lfloor \frac{r_{bi}}{c} \frac{1}{PRI} \right\rfloor, \tag{1}$$

where c is the speed of light, PRI is the pulse repetition interval and $\lfloor \cdot \rfloor$ denotes the floor function, i.e., the largest integer not greater than the argument of the function. All subsequent pulses forwarded to the Tx satellite will have the synchronization signal and radar echoes superimposed, overcoming the need to build another RF link between the Tx and Rx satellites for the synchronization signal.

The up-conversion, i.e., $+\Delta f$ and the down-conversion, i.e., $-\Delta f$ (see upper panel in Fig. 2) are performed by independent oscillators resulting in phase errors. The instantaneous phase of an oscillator can be modeled as [14]:

$$\varphi_{osc}(t) = 2\pi f_{osc} t + \varphi_{st}(t) + \varphi_0, \tag{2}$$

where f_{osc} is the frequency of the oscillator (or its expected value, since the frequency itself is a random variable), φ_0 is a constant arbitrary phase and $\varphi_{st}(t)$ is a time-varying phase error. This phase error, also known as phase noise, is a random process and is often modeled by a second-order stationary stochastic process, which is conveniently characterized in the Fourier frequency domain by its power spectral density (PSD), $S_{\varphi_{st}}(f)$, where f is the frequency offset from f_{osc} [12]. Based on (2) the phase errors on the Tx side after the frequency shift reversing, (i.e., $-\Delta f$), at nominal RF frequency can be modeled as:

$$\varphi_e(t) = 2\pi\delta f t + M\varphi_{st_{Tx}}(t) - M\varphi_{st_{Rx}}(t - \Delta t_{Rx-Tx}), \tag{3}$$

where δf indicates a frequency offset produced by non-identical stable local oscillators (STALO) frequencies, $M = \Delta f / f_{osc}$ is the ratio of RF to master oscillator frequency, Δt_{Rx-Tx} is the time delay in the MirroSAR link (see upper panel of Fig. 2),i.e., between the transmission of the superimposed signals from Rx satellite and their reception by the Tx satellite, $\varphi_{st_{Tx}}(t)$ and $\varphi_{st_{Rx}}(t - \Delta t_{Rx-Tx})$ are the random phase errors of the Tx satellite and Rx satellite oscillators at time t and $t - \Delta t_{Rx-Tx}$, respectively. Assuming uncorrelated oscillators with equal PSD, $S_{\varphi_{st}}(f)$, we can model these phase errors in (3) as:

$$\varphi_e(t) = 2\pi\delta f t + \varphi_{st}(t) \tag{4}$$

where

$$\varphi_{st}(t) = M\varphi_{st_{Tx}}(t) - M\varphi_{st_{Rx}}(t - \Delta t_{Rx-Tx}) \tag{5}$$

is a random process with PSD equal to $2MS_{\varphi_{st}}(f)$. It is important to notice that these phase errors $\varphi_e(t)$ will be the same for the synchronization signal and the radar echo as the up-conversion $+\Delta f$ and down-conversion $-\Delta f$ is applied to the superimposed signal.

The overlaid signal is then down-converted to baseband using the same LO that generated the transmitted radar pulses. Due to a filtering effect known as range correlation, the low-frequency components of the phase noise of the LO (low-frequency components of $\varphi_{st}(t)$ in (2)) are cancelled, similar to monostatic SAR systems. This filtering effect behaves as high-pass filter and is caused by correlation between the phase noise on the LO signal and the phase noise on the received signal, in this case, the overlaid signal, which is the sum of the synchronization signal and the radar echo. The amount of correlation, and consequently the amount of filtering, is determined by the time delay between the transmitted and received signals. Because the correlation of the transmitted signal phase noise with the oscillator phase noise at the

receiving time is strongest for short time delays, the amount of filtering is large at short time delays and become smaller as time delay increases. The remaining high-frequency phase noise components $\varphi_{st_{HF}}(t)$ will have a PSD equal to $2S_{\varphi_{st}}(f)(1-\cos(2\pi f\Delta t))$ where Δt is the time delay. As previously noted, there are differences in the time delays involved in receiving the synchronization signal, which depends on the two-way distance between the Rx and Tx satellites, and radar echo, which depends on the bistatic range. Consequently, the quantity of low-frequency components canceled for the synchronization signal differs from that for radar echo; it is greater for the synchronization signal. This results in different $\varphi_{st_{HF}}(t)$ terms for the synchronization signal and radar echo. However, it is worth mentioning, that $\varphi_{st_{HF}}(t)$ is negligible in comparison to the $\varphi_e(t)$ in (4). Therefore, we may state that the total phase errors on the synchronization signal and radar echoes caused by the involved oscillators following the demodulation to baseband, are equal to $\varphi_e(t)$.

B. On-ground

The extraction of the synchronization signal and the radar echo is performed in the range-Doppler domain after the data (synchronization signal + radar echo) has been range compressed. The transformation to the range-Doppler domain is carried out in blocks, as schematically depicted in Fig. 3.This block-based approach enables accurate "tracking" of the location of the range-compressed synchronization signal within the range-Doppler domain. If the distance between the Tx and Rx satellites is constant over the data taken, i.e., $d_{Tx-Rx}(t) = d_{Tx-Rx}$ and the frequency offset between the oscillators in (4) is zero, i.e., $\delta f = 0$, the range compressed synchronization signal, unlike the range compressed SAR data, will show a strong peak in the range-Doppler domain at Doppler frequency zero and at a range equal to d_{Tx-Rx}. However, in reality, the Tx-Rx satellites distance varies during the data taken, $d_{Tx-Rx}(t) \neq d_{Tx-Rx}$, and there is a non-zero frequency offset. This implies that the range compressed synchronization signal in the range- Doppler domain will present a strong peak around a Doppler frequency equal to

$$f_{Dopp} = \delta f - \frac{v_{Tx-Rx}}{c}\left(2f_{0_{Tx}} + \Delta f\right), \tag{6}$$

where $f_{0_{Tx}}$ is the carrier frequency of the Tx satellite and v_{Tx-Rx} is the relative velocity between the two satellites. Dual-frequency GNSS (Global navigation satellite system) receivers on satellites and ground-based orbit determination systems can provide few mm/s accuracy (1-sigma) for the v_{Tx-Rx}. This accuracy level allows us to determine the second component of f_{Dopp} (6) with an accuracy of less than 1 Hz for an X-band SAR system. To estimate the frequency offset δf of the two oscillators, we will use the $N_{synch_{only}}$ pulses defined in (1), which only have the synchronization signal, as illustrated in the left part of Fig. 3. Following range compression of the $N_{scynch_{only}}$ pulses, the Doppler frequency f_{Dopp} is estimated using the Discrete Time Fourier Transform, and δf is computed using (6). This will be then exploit in the next step. The accuracy of estimating f_{Dopp} depends on the thermal noise level, i.e., the synchronization signal to noise ratio, the number of $N_{synch_{only}}$ pulses and the phase noise, i.e., $\varphi_{st}(t)$ of the oscillator.

Once the value of f_{Dopp} in (6) is determined, a narrow range-Doppler filter will be employed around f_{Dopp} for the first block of data. The width of the range-Doppler filter in the Doppler domain is influenced by the size of the block, the variation of Doppler frequency resulting from v_{Tx-Rx} within the processed block and the frequency stability of the oscillators. For instance, Fig. 4(a) shows the baseline distance between the HRWS satellite (Tx satellite) and the three Rx satellites as a function of the argument of latitude for the HRWS mission [20]-[21]. Fig. 4 (b) shows the relative velocity between the HRWS satellite and the three Rx satellites. We note that the satellite distance variation is less than 1.5 m/s. Fig. 4 (c) shows the corresponding Doppler component (second addend of (6)) as function of the argument of latitude.

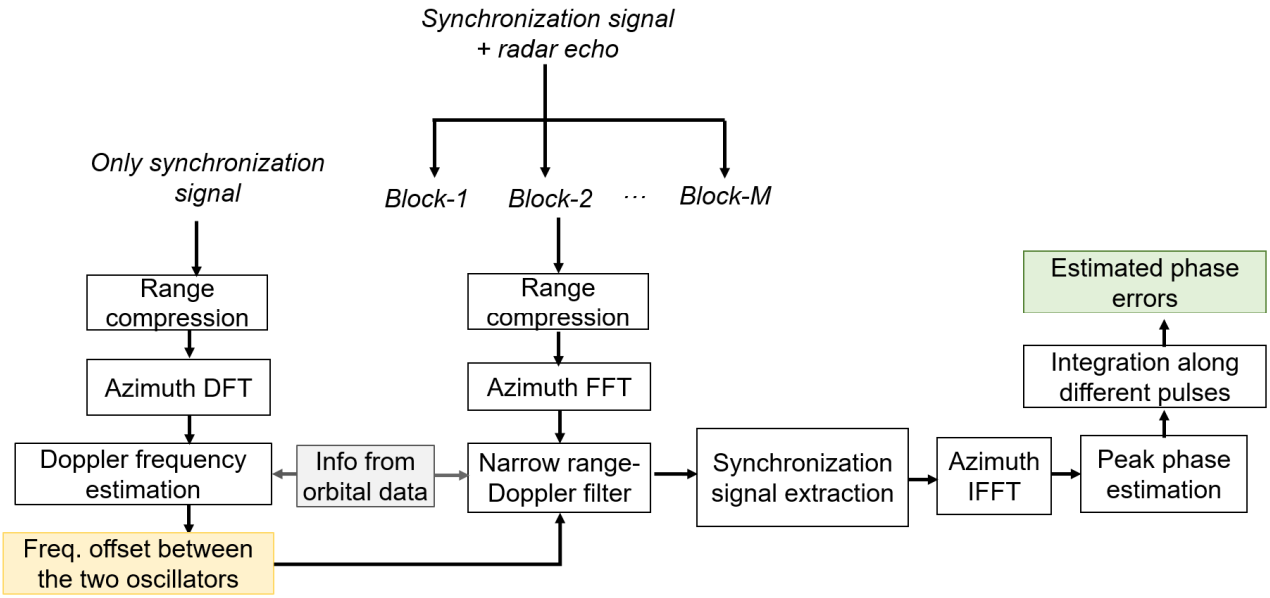

Fig. 3 Block diagram of the extraction of the synchronization signal from the radar echo and estimation of the phase errors.

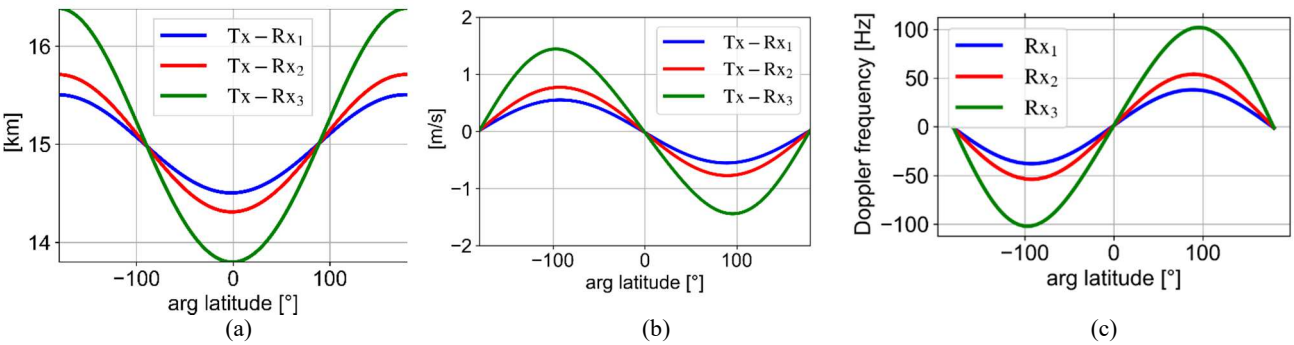

(a) (b) (c)

Fig. 4 (a) Distance between HRWS satellite and the three Rx satellites as function of the argument of latitude and (b) relative velocity between the two satellites as function of the argument of latitude and (c) Doppler frequency variation as function of the argument of latitude.

The synchronization signal, once extracted, is transformed back into the azimuth time domain. Subsequently, the phase of the compressed peak for each pulse is estimated, assuming a constant phase within the main lobe. If the synchronization signal is a copy of the chirp signal transmitted to the ground, it can be shown that the phase of the peak of the range compressed synchronization signal is:

$$\varphi_{peak}(t) = -4\pi \frac{f_{0_{TX}}}{c} d_{Tx-Rx}(t) - 2\pi \frac{\Delta f}{c} d_{Tx-Rx}(t) + 2\pi\delta f t + \varphi_{st}(t) \quad (7)$$

where $f_{0_{TX}}$ is the carrier frequency. Therefore, estimating the peak phase enables us to estimate the $\varphi_{st}(t)$ component of the phase error in (4). Due to the lower power of the synchronization signal compared to the radar echo, it is necessary to integrate the phase errors from the different pulses. Then, the estimated phase errors are corrected in the radar echo data.

Finally, the range decompression is performed to the extracted synchronization signal and the derived synchronization signal can be coherently subtracted from the radar data before performing the SAR image processing. The subtraction creates a gap in the Doppler spectrum that depends on the width of the applied filter for a specific range [18]. To mitigate any impact on the received SAR data from the ground due to the removal of the synchronization signal, the transmitted synchronization signal can be phase-modulated by a constant phase term, shifting the synchronization signal outside the processed Doppler bandwidth.

It is important to note that although only one Rx satellite is illustrated in Fig. 2 for simplicity, the proposed synchronization scheme can simply be generalized to the case of several Rx satellites. The frequency shift $+\Delta f$ will be different for each Rx satellite in order to avoid interference between the radar echoes from the different satellites. The transmitting satellite may have a larger bandwidth in order to accommodate the radar echoes received by all the Rx satellites.

III. End-to-end Analysis with TerraSAR-X Data

In this section an end-to-end simulation of the proposed synchronization scheme using real TerraSAR-X data is shown. Fig. 5 shows the focused TerraSAR-X image of the Munich urban area taken under consideration. A synchronization signal, assumed to be an up-chirp signal with a 20 µs pulse length, and synchronization signal-to-radar echo ratios of -5 dB and -7 dB, along with phase errors as defined in (4) for the same ultrastable oscillator as in [12], was added to the raw TerraSAR X data. The synchronization approach discussed in Section II is then performed to the data. A bistatic distance of 700 km and a PRF = 3300 Hz is assumed which result in 20 traveling pulses, from which δf is estimated. It assumed here that the distance between the two satellites during the data taken is equal to 1.5 m/s. Following the range compression and the transformation in the range-Doppler domain of the superimposed raw TerraSAR-X data and synchronization signal, a range-Doppler filter around $f_{Dopp} = -100$ Hz is applied. After the extraction of the reference signal, the phase of the peak for each compressed pulse is estimated.

Fig. 6 and Fig. 7 compares the retrieved phase noise from the estimated peak phase by exploiting (9) (red curve) with the simulated phase noise (blue curve) when the synchronization signal to radar echo power ratio is equal to -5 dB and -7 dB, respectively. Furthermore, the estimated phase errors are integrated across different pulses. Fig. 8 shows the accuracy of phase noise estimation as a function of the integrated pulses. We note, for a synchronization signal to radar echo power ratio of -5 dB, the achievable accuracy is approximately 0.7° for N = 250 pulses, while for a ratio of -7 dB, it is approximately 0.9° with N = 270 pulses. In both cases, an accuracy of less than 1° in phase error estimation is guaranteed.

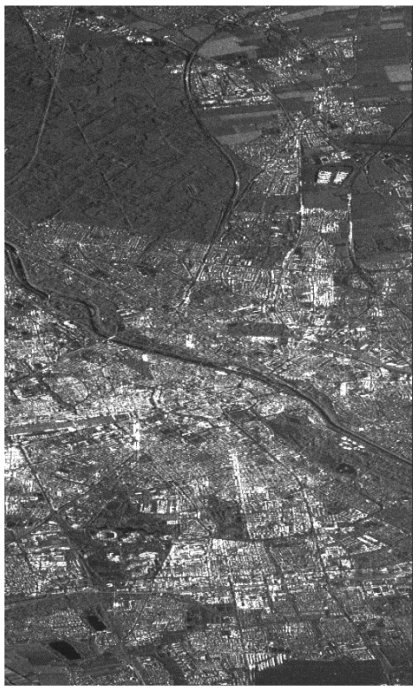

Fig. 5 TerraSAR-X image over Munich urban area.

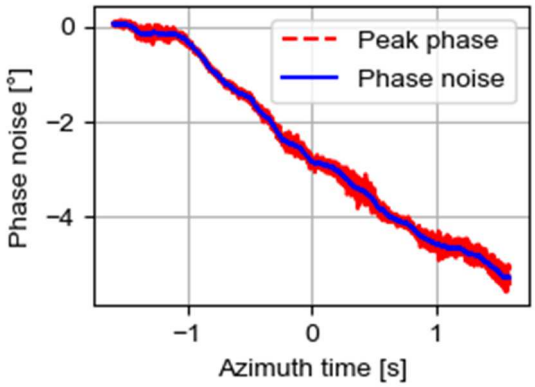

Fig. 6 Comparison between the estimated phase noise from the peak phase and the simulated phase noise for the ultrastable oscillator in [12] when the synchronization signal to radar echo ratio is – 5dB.

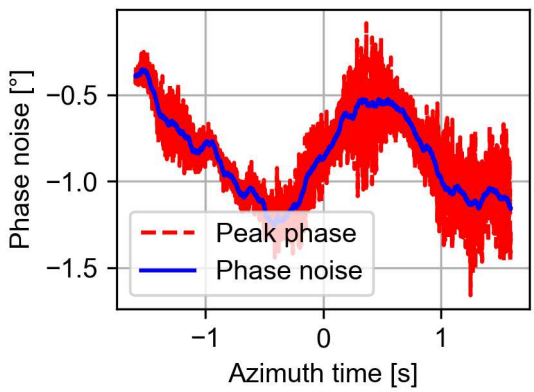

Fig. 7 Comparison between the estimated phase noise from the peak phase and the simulated phase noise for the ultrastable oscillator in [12] when the synchronization signal to radar echo ratio is – 7dB.

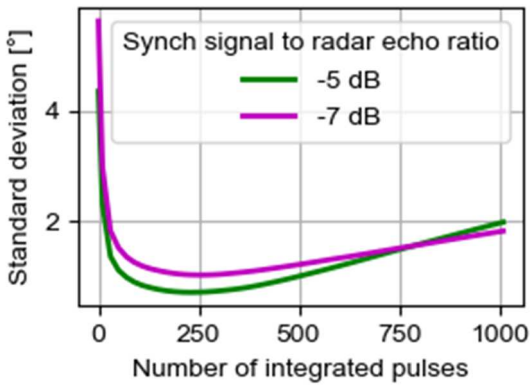

Fig. 8 Phase noise estimation accuracy as function of the number of integrated pulses.

IV. Conclusions

In this paper a phase synchronization technique based on microwave link is investigated within the MirrorSAR concept. The accuracy of the proposed technique has been evaluated through simulations using real TerraSAR-X data. We demonstrated that even when the synchronization signal-to-radar echo ratio is as low as -7 dB, the proposed synchronization technique guarantees phase error estimations with an accuracy of less than 1°.

References

[1] A. Moreira, P. Prats-Iraola, M. Younis, G. Krieger, I. Hajnsek and K. P. Papathanassiou, "A tutorial on synthetic aperture radar," in *IEEE Geoscience and Remote Sensing Magazine*, vol. 1, no. 1, pp. 6-43, March 2013.

[2] D. Massonnet, "Capabilities and Limitations of the Interferometric Cartwheel," *IEEE Transactions on Geoscience and Remote Sensing*, Vol. 39, No. 3, pp. 506-520, Mar 2001.

[3] G. Krieger, A. Moreira, "Multistatic SAR Satellite Formations: Potentials and Challenges," *Proc. IGARSS*, Seoul, Korea, 2005.

[4] M. Zink et al., "TanDEM-X: The New Global DEM Takes Shape," *IEEE Geosci. RemoteSens. Mag*., Vol. 2, 2014.

[5] P. Dubois-Fernandez, H. Cantalloube, B. Vaizan, G. Krieger, R. Horn, M. Wendler, and V. Giroux, "ONERA-DLR bistatic SAR campaign: Planning, data acquisition, and first analysis of bistatic scattering behavior of natural and urban targets," P*roc. Inst. Elect. Eng.—Radar, Sonar Navig*., vol. 153, no. 3, pp. 214–223, Jun. 2006.

[6] D. Martinsek and R. Goldstein, "Bistatic radar experiment," *in Proc. EUSAR*, Friedrichshafen, Germany, 1998, pp. 31–33.

[7] J. Ender, I. Walterscheid, and A. Brenner, "New aspects of bistatic SAR: Processing and experiments," *in Proc. IGARSS*, Anchorage, AK, 2004, pp. 1758–1762.

[8] G. Yates, A. Horne, A. Blake, R. Middleton, and D. Andre, "Bistatic SAR image formation," *in Proc. EUSAR*, Ulm, Germany, 2004, pp. 581–584.

[9] J. L. Auterman, "Phase stability requirements for a bistatic SAR*," in Proc. IEEE Nat. Radar Conf*., Atlanta, GA, 1984, pp. 48–52.

[10] M. Eineder, "Oscillator clock drift compensation in bistatic interferometric SAR," *in Proc. IGARSS*, Toulouse, France, 2003, pp. 1449–1451.

[11] M. Weiß, "Time and frequency synchronisation aspects for bistatic SAR systems," *in Proc. EUSAR*, 2004, pp. 395–398.

[12] G. Krieger and M. Younis, "Impact of oscillator noise in bistatic and multistatic SAR," *IEEE Geoscience and Remote Sensing Letters*, vol. 3, no. 3, pp. 424-428, July 2006.

[13] M. Younis, R. Metzig and G. Krieger, "Performance prediction of a phase synchronization link for bistatic SAR," *IEEE Geoscience and Remote Sensing Letters*, vol. 3, no. 3, pp. 429-433, July 2006.

[14] P. Lopez-Dekker, J. J. Mallorqui, P. Serra-Morales and J. Sanz-Marcos, "Phase Synchronization and Doppler Centroid Estimation in Fixed Receiver Bistatic SAR Systems," *IEEE Transactions on Geoscience and Remote Sensing*, vol. 46, no. 11, pp. 3459-3471, Nov. 2008

[15] Z. He, F. He, J. Chen, H. Huang, Z. Dong and D. Liang, "Echo-Domain Phase Synchronization Algorithm for Bistatic SAR in Alternating Bistatic/Ping–Pong Mode," *IEEE Geoscience and Remote Sensing Letters*, vol. 9, no. 4, pp. 604-608, July 2012.

[16] E. Rodrigues-Silva and M. Rodriguez-Cassola, "Analysis of a POD-based Approach for Phase and Time Synchronization of Bistatic and Multistatic SAR Systems," *EUSAR 2021; 13th European Conference on Synthetic Aperture Radar*, 2021, pp. 1-6.

[17] G. Krieger *et al*., "TanDEM-X: A Satellite Formation for High-Resolution SAR Interferometry," *IEEE Transactions on Geoscience and Remote Sensing*, vol. 45, no. 11, pp. 3317-3341, Nov. 2007.

[18] G. Krieger, M. Zonno, J. Mittermayer, A. Moreira, S. Huber and M. Rodriguez-Cassola, "MirrorSAR: A Fractionated Space Transponder Concept for the Implementation of Low-Cost Multistatic SAR Missions," *EUSAR 2018.*

[19] G. Krieger *et al*., "MirrorSAR: A fractionated space radar for bistatic, multistatic and high-resolution wide-swath SAR imaging," *2017 IEEE International Geoscience and Remote Sensing Symposium (IGARSS)*, 2017, pp. 149-152.

[20] J. Janoth, M. Jochum, L. Petrat, and T. Knigge, "High Resolution Wide Swath – the next Generation X-band mission", *Proc. of IGARSS 2019*.

[21] M. Bartusch, A. Nuncio Quiroz, S. Stettner, A. Moreira, and M. Zink, "German X-band Spaceborne SAR Heritage and the Future HRWS Mission", *in Proc. IGARSS*, Brussels, Belgium, 2021.

[22] J. Mittermayer *et al*., "MirrorSAR: An HRWS Add-On for Single-Pass Multi-Baseline SAR Interferometry," *IEEE Transactions on Geoscience and Remote Sensing*, vol. 60, pp. 1-18, 2022.